Advanced Functional Materials

MoS2@NiO composite nanostructures: an advanced nonprecious catalyst for hydrogen evolution reaction in alkaline media

--Manuscript Draft--

Manuscript Number:	adfm.201807562
Full Title:	MoS2@NiO composite nanostructures: an advanced nonprecious catalyst for hydrogen evolution reaction in alkaline media
Article Type:	Full Paper
Section/Category:	
Keywords:	
Corresponding Author:	Alberto Vomiero Lulea Tekniska Universitet Lulea, SWEDEN
Additional Information:	
Question	**Response**
Please submit a plain text version of your cover letter here.	Luleå, 26/10/2018 To Dr. Joern Ritterbusch Editor in chief Advanced Functional Materials Re: Submission of the Manuscript entitled “MoS2@NiO composite nanostructures: an advanced nonprecious catalyst for hydrogen evolution reaction in alkaline media” for consideration as an article in Advanced Functional Materials. Dear Dr. Joern Ritterbusch, We are hereby submitting the manuscript entitled “MoS2@NiO composite nanostructures: an advanced nonprecious catalyst for hydrogen evolution reaction in alkaline media” by Zafar Hussain Ibupoto, Aneela Tahira, PengYi Tang, Xianjie Liu, Joan Ramon Morante, Mats Fahlman, Jordi Arbiol, Mikhail Vagin, Alberto Vomiero, to be considered for publication as an article in Advanced Functional Materials. Water electrolysis is one of the most promising ways for oxygen and hydrogen production via simple, cheap and environmentally compatible methodology. For the purpose, noble metal catalysts, i.e. Pt-based electrodes for hydrogen are the most efficient systems. However, they are incompatible with practical exploitation, due to their high cost and scarcity in nature. For this reason, the researchers are pushing the development of alternative catalysts composed of cheap and environmentally friendly materials, to be prepared through simple and scalable methodologies. The main challenge in the field is to be able to produce catalysts, which work for hydrogen production with performance comparable or better than noble metal-based catalysts in terms of onset potential, overpotential, Tafel slope (i.e. the variation of current density with the external applied potential) and long-term stability.

	Here we propose the synthesis of composite materials for hydrogen evolution reaction (HER) in alkaline media via simple and scalable methodology. While NiO and MoS2 nanostructures have been separately investigated for HER, their poor performance does not allow their practical exploitation. Specifically, the main bottleneck in functionality lies in the low density of active sites in pristine NiO and MoS2, which limits their performance. To overcome this issue we propose here an advanced composite system based on NiO nanostructured film acting as fast charge transporter, coated with a highly porous MoSx layer, which exhibits a high density of catalytically active edges. The combination of the charge transport in NiO and the high catalytic activity of the sulfide top layer makes the proposed heterostructures effective for HER, with 226 mV overpotential to achieve current density of 10 mA/cm2. The Tafel slope of 43 mV dec-1 is the lowest possible in alkaline media for non-precious catalyst to date and it is very close to Pt/C-based catalysts, revealing that the HER kinetics is highly favorable at the surface of the MoS2@NiO composite. In terms of Tafel slope, the performance of the new catalyst is comparable to that of Pt/C in alkaline media. Additionally, the top MoSx layer can protect the oxide under-layer from dissolution, resulting in long-term stability of the system, with current density kept unvaried after 13 hours operations. We are convinced that these results represent a major advancement in the design of functional catalysts as well as newly composite material, and can inspire research in correlated disciplines, where different functionalities (like catalytic activity, charge transport, resistance in harsh environment) are demanded, like, for instance, in photocatalysis, photoelectrochemical cells, lithium ion batteries, or supercapacitors. For all these reasons, we are confident that this manuscript can be of interest for the broad readership of Advanced Functional Materials. Looking forward to your positive evaluation. Yours sincerely, Alberto Vomiero, Ph.D. FRSC (UK), FIMMM, FInstP, FIoN, Marie Curie IOF, Member of the Global Young Academy Swedish Foundations' Consolidator Grant Fellow (http://startinggrant.se/) Associate Editor of Nano Energy (Elsevier) Editorial Board of Scientific Reports (NPG) Associate Editor of the Journal Materials for Renewable and Sustainable Energy (Springer) Chair in Experimental Physics Division of Materials Science Department of Engineering Science and Mathematics Luleå University of Technology SE-971 98 Luleå, Sweden e - mail alberto.vomiero@ltu.se
Do you or any of your co-authors have a conflict of interest to declare?	No. The authors declare no conflict of interest.
Corresponding Author Secondary Information:	

Corresponding Author's Institution:	Lulea Tekniska Universitet
Corresponding Author's Secondary Institution:	
First Author:	Zafar Hussain Ibupoto
First Author Secondary Information:	
Order of Authors:	Zafar Hussain Ibupoto
	Aneela Tahira
	PengYi Tang
	Xianjie Liu
	Joan Morante
	Mats Fahlman
	Jordi Arbiol
	Mikhail Vagin
	Alberto Vomiero
Order of Authors Secondary Information:	
Abstract:	The design of the Earth abundant, non-precious, efficient and stable electrocatalysts for efficient hydrogen evolution reaction in alkaline media is a hot research topic in the field of renewable energies. Here we propose a heterostructured system composed of MoSx deposited on NiO nanostructures (MoS2@NiO) as robust catalyst for water splitting. NiO nanosponges are applied as co-catalyst for MoS2 in alkaline media. Both NiO and MoS2@NiO composites are prepared by a hydrothermal method. The NiO nanostructures exhibit sponge-like morphology and are completely covered by the sheet-like MoS2. The NiO and MoS2 exhibit cubic and hexagonal phases, respectively. In the MoS2@NiO composite, the hydrogen evolution reaction experiment in 1M KOH electrolyte resulted in an extremely low overpotential (226 mV) to produce 10 mA cm-2 current density. The Tafel slope for that case is 43 mV/decade, which is the lowest ever achieved for MoS2-based electrocatalyst in alkaline media. The catalyst is highly stable for at least 13 hours, with no decrease in the current density. This simple, cost effective and environmentally friendly methodology can pave the way for exploitation of MoS2@NiO composite catalysts not only for water splitting, but also for other applications such as lithium ion batteries, and fuel cells.

MoS_2@NiO composite nanostructures: an advanced nonprecious catalyst for hydrogen evolution reaction in alkaline media

Zafar Hussain Ibupoto[a, b*], Aneela Tahira[a], PengYi Tang[c,d], Xianjie Liu[e], Joan Ramon Morante[d], Mats Fahlman[e], Jordi Arbiol[c,f], Mikhail Vagin[e], Alberto Vomiero[a*]

[a] Division of Material Science, Department of Engineering Sciences and Mathematics, Luleå University of Technology, 97187 Luleå, Sweden

[b] Dr. M.A Kazi Institute of Chemistry University of Sindh Jamshoro, 76080, Sindh Pakistan

[c] Catalan Institute of Nanoscience and Nanotechnology (ICN2), CSIC and BIST, Campus UAB, Bellaterra, 08193 Barcelona, Catalonia, Spain

[d] Catalonia Institute for Energy Research (IREC), Jardins de les Dones de Negre 1, Sant Adrià del Besòs, Barcelona 08930, Catalonia, Spain

[e] Department of Physics, Chemistry and Biology, Linkoping University, 58183 Linkoping, Sweden

[f] ICREA, Pg. Lluís Companys 23, 08010 Barcelona, Catalonia, Spain

* Corresponding authors: Zafar Hussain Ibupoto, Alberto Vomiero
Email: alberto.vomiero@ltu.se, zafar.ibupoto@ltu.se

Abstract

The design of the Earth abundant, non-precious, efficient and stable electrocatalysts for efficient hydrogen evolution reaction in alkaline media is a hot research topic in the field of renewable energies. Here we propose a heterostructured system composed of MoS_x deposited on NiO nanostructures (MoS_2@NiO) as robust catalyst for water splitting. NiO nanosponges are applied as co-catalyst for MoS_2 in alkaline media. Both NiO and MoS_2@NiO composites are prepared by a hydrothermal method. The NiO nanostructures exhibit sponge-like morphology and are completely covered by the sheet-like MoS_2. The NiO and MoS_2 exhibit cubic and hexagonal phases, respectively. In the MoS_2@NiO composite, the hydrogen evolution reaction experiment in 1M KOH electrolyte resulted in an extremely low overpotential (226 mV) to produce 10 mA cm^{-2} current density. The Tafel slope for that case is 43 mV/decade, which is the lowest ever achieved for MoS_2-based electrocatalyst in alkaline media. The catalyst is highly stable for at least 13 hours, with no decrease in the current density. This simple, cost effective and environmentally friendly

methodology can pave the way for exploitation of MoS_2@NiO composite catalysts not only for water splitting, but also for other applications such as lithium ion batteries, and fuel cells.

Text

Hydrogen production by cost-effective electrochemical water splitting is one of the most promising approaches to confront the energy crisis and to obtain clean fuels with high energy density. Hydrogen evolution reaction (HER) aims at meeting the stringent criteria for entering the energy market, through fabrication of electro-catalysts guaranteeing highly efficient hydrogen production.[1,2] However, the best-known electro-catalysts for hydrogen production are Pt and Pt-derivatives, which hinder the possibility of application of such technology due to their high cost and scarcity.[3,4] Therefore, the development of environmentally friendly, low cost and Earth-abundant catalysts to replace noble metals is mandatory to realize large scale electro-catalytic hydrogen production.[5]

To obtain efficient water splitting at a practical level, the electrocatalysts for HER must work either in acidic or in alkaline electrolytes at low overpotential.[6] To develop simple and cost effective functional catalysts for electrochemical water splitting, the latest research directions involve the investigation of Mo-based nanomaterials,[7] including Mo_2C, [8, 9, 10, 11, 12] MoN,[13] MoS_2 ,[14] and related compounds,[15,16,17] aiming at competing with Pt in terms of catalytic efficiency in HER. A successful strategy is the deposition of Mo compounds on various conducting substrates with high specific surface area, including carbon nanosheets,[18] and nanotubes,[19,20] which prevent aggregation of the nanocomposites, keeping the effect of the high density of their active sites.

HER performance of Mo-compounds is critically dependent on the crystalline planes exposed to the catalytic activity. For example, in MoS_2, (10-10) edges are highly catalytically active, while (0001) basal planes are inert.[21] This observation is driving the research on the development of new materials with limited flat surfaces and increased density of edge sites, such as crystalline,[22, 23, 24, 25] amorphous compounds [26, 27, 28] and hybrid systems.[29, 30, 31] Researchers also reported recently that strain induced by patterned gold nanocones can activate the basal plane of monolayer 2H-MoS_2 for HER.[32] However, despite the promising results, Mo-compounds are still below the expectations in terms of functional properties, compared to Pt.

In parallel to Mo-compounds, other novel electro-catalysts were recently introduced for HER based on Earth-abundant metal chalcogenides.[2] A successful strategy to boost functional performances is the application of heterostructured nanomaterials: for example, decoration with Ni/NiO nanoparticles of $CoSe_2$ nanobelts (on a stable glassy carbon electrode) demonstrate improved HER,[33] mainly due to the chemical coupling effect of $CoSe_2$ and of the anchored Ni/NiO.

Besides this, the fabrication of catalysts for HER typically needs several successive steps, making the development of a functional electrocatalyst with enhanced HER activity in alkaline media for industrial application a very challenging task to date. NiO electrocatalyst exhibits poor HER performance, due to both the low electrical conductivity and the poor catalytic activity.

For these reasons, aiming at increasing the density of active sites and the electrical conductivity, we propose the development of a MoS_2@NiO composite nanostructure, targeting the fabrication of a highly stable and efficient electrocatalyst for HER in alkaline media. Herein, we report a new class of heterostructure materials as robust catalyst for HER in 1M KOH at room temperature. The electrocatalyst is based on a MoS_2@NiO composite structure that reveal an efficient HER activity due to synergetic effect between MoS_2 and NiO as supporting co-catalyst material. This composite electrode exhibits excellent performance for HER with a Tafel slope (43 mV/decade) comparable to that of commercial Pt/C and compatible with practical applications. Importantly, the presented electrocatalyst is highly stable with negligible loss of potential for almost 10 hours under operation. These results can be of importance not only for water splitting but also for other processes and fields of energy sector, in which new electro-catalysts can improve device functionality, like, for instance, in lithium ion batteries, supercapacitors and fuel cells.

Figure 1(a) shows the morphological features of NiO, revealing a porous and flower like shape. After the deposition of the MoS_2 layer (**Figure 1**(b)), the composite nanostructures have porous nanoparticle morphology. SEM/TEM images of pristine MoS_2 (**Figure S1**) indicate a nanosheet-like morphology.

XRD analysis (**Figure 1)** of pure NiO confirms its cubic phase (diffraction pattern well matching the JCPDS card no. 96-101-0382). After MoS_x deposition, the MoS_2@NiO composite exhibits reflections fully compatible with NiS cubic phase (JCPDS card no. 96-591-0138), in addition to reflections from the NiO cubic phase.

To probe the chemical composition, X-ray photoelectron spectroscopy (XPS) studies were carried out. Survey scans were used to obtain the elemental composition (see Tables S1-S3 for XPS quantitative analysis). In the MoS_2@NiO sample, the Mo:S:O:Ni atomic ratio measured from XPS is equal to 26.5:34.0:36.5:3.0. The low Ni concentration is ascribed to the small signal coming from the underlying NiO layer, suggesting a nearly complete coverage of the NiO nanostructures by the MoS_2 layer. The high concentration of oxygen (36.5% at.) indicates that Mo is partially

oxidized, as indicated by TEM, suggesting that the NiO underlying layer is covered by a mixture of molybdenum sulfides and oxide.

In **Figure 1**(e) the S2p core level spectrum for MoS_2@NiO is reported. The MoS_2@NiO contains two spin-split doublets ($S2p_{3/2}$ and $S2p_{1/2}$) with a 4:1 ratio. The high intensity $S2p_{3/2}$ peak is situated at ~161.5 eV and the second lower intensity feature is located at ~163.0 eV. The main S2p core level feature for the composite system can be assigned to S^{2-}.[34, 35, 36] It is suggested that the shift of the S2p core level to lower binding energy from ~162.2 eV to ~161 eV is indicative of a transition from 2H to 1T phase of MoS_2. In **Figure 1**(f) the Mo3d and S2 core level spectrum for MoS_2@NiO is reported. The Mo3d spectrum of the MoS_2@NiO sample contains three spin-split doublets ($Mo3d_{5/2}$ and $Mo3d_{3/2}$) with the $Mo3d_{5/2}$ peaks centered at ~228.7 eV (54%), ~230.0 eV (24%) and ~232.4 eV (22%). The feature at 228.7 eV can be assigned to Mo^{4+} and is compatible with the binding energy of the 1T phase of MoS_2.[34] The higher binding energy features are assigned to Mo^{5+} and Mo^{6+} respectively, in good agreement with literature values.[35] As the Mo^{5+} and Mo^{6+} features are not present in stoichiometric MoS_2 films, we expect that they originate from MoO_y or MoS_xO_y regions in the films. For MoS_2@NiO the relative concentration of the oxygen-derived (Mo^{5+}, Mo^{6+}) components is about 50%, in good agreement with the stoichiometric values previously reported.

The chemical composition, the morphology and crystalline features were also analyzed via high angle annular dark field (HAADF) scanning transmission electron microscopy (STEM) combined with electron energy loss spectroscopy and high-resolution transmission electron microscopy (HRTEM) for both the samples (**Figure 2**). The pure NiO sample is composed of Ni and O and no other impurity was detected. Furthermore, HRTEM confirms that the material crystallizes in the cubic NiO phase, [FM3-M]-Space group 225, with lattice parameters of a = b= c = 0.4179 nm, and $\alpha = \beta = \gamma = 90°$, as visualized along the [101] direction.

In the MoS_2@NiO sample, the presence of Ni, O, Mo, and S was confirmed in the composite. The HRTEM and the corresponding FFT spectrum indicate that the nanoplates crystallize in the cubic NiO phase, [FM3-M]-Space group 225, with lattice parameters of a = b= c = 0.4179 nm, and $\alpha = \beta = \gamma = 90°$ as visualized along the [110] direction. The detailed structure of the NiO/MoS_x interface and the corresponding FFT spectrum indicate that it crystallizes in the hexagonal MoS_2 phase, [P63/MMC]-Space group 194, with lattice parameters of a = b = 0.3165 nm, c = 1.2295 nm, and $\alpha = \beta = 90°$, $\gamma = 120°$ as visualized along the [1-21-3] direction.

These results are in good agreement with XRD and XPS.

Figure 3(a) shows the polarization curves obtained through linear sweep voltammetry (LSV) electrochemical mode for the various electrocatalysts: pristine GCE, MoS_2, NiO, MoS_2@NiO, and benchmark 20%Pt/C at scan rate of 5 mV/s in 1M KOH solution saturated with N_2 gas. The GCE shows HER activity at higher potential (~570 mV vs RHE), compared to all the other samples. The nanostructured MoS_2 exhibits HER activity still at high potential (~508 mV vs RHE), which can probably due to the fact that MoS_2 tends to agglomerate during HER experiment, resulting in low density of active edges and thus in poor HER performance. The catalytic activity of NiO is also limited and HER activity is reported at high potential (~535 mV vs RHE). The composite system, instead, exhibits HER activity at low dynamic potential: the MoS_2@NiO composite system achieves 10 mA/cm^2 current density at 406 mV overpotential. This behavior can be assigned to the synergetic effect of the MoS_2 nanosheets on the surface of NiO nanostructures, which increases the density of active edges (thanks to MoS_2), and the fast charge transfer guaranteed by the NiO nanostructures. The overpotential for the MoS_2@NiO electrocatalyst is close or lower than the reported electrocatalysts such CoP/CC (500 mV),[37] N, P-G (700 mV),[38] MoSx (540 mV),[25] Co-S/FTO (480 mV),[39] and Co-NR CNTs (450 mV).[40] The overpotential of noble Pt/C catalyst is about 110 mV, of course lower than MoS_2@NiO, but still the reported results for a nonprecious and earth abundant electrocatalyst can be valuable to develop new nanomaterials for water spitting. These results indicate superior performance for the composite system than for the pure NiO and MoS_2 catalysts.

Entering into the investigation of the HER process, the HER kinetics can be evaluated from the linear regions of the Tafel plot, through fitting the LSV curves with the Tafel equation [Eq. (1)]:

$$\eta = b \log(j) + a \qquad (1)$$

Where *a* is related to the exchange current density (j_0) and *b* represents the Tafel slope. In alkaline conditions, the HER kinetics most likely takes place via the formation of hydrogen adsorbed intermediates (H_{ads}). The formation of H_{ads} involves electron transfer via the discharge of water by following the Volmer step [Eq. (2)]:

$$H_2O + e^- \rightarrow H_{ads} + OH^- \qquad (2)$$

The next step in HER is either through a second electron transfer (known as Heyrovsky step [Eq. (3)]):

$$H_{ads} + H_2O + e^- \rightarrow H_2 + OH^- \quad (3)$$

or by the Tafel step [Eq. (4)]:

$$H_{ads} + H_{ads} \rightarrow H_2 \quad (4)$$

Generally, a Tafel slope of 120, 40, and 30 mV/decade correspond to the Volmer, Heyrovsky, or Tafel step as the rate-limiting and determining step in the HER kinetics, respectively.[41, 42, 43] The Tafel slope of 43 mV/decade suggests that the Heyrovsky step is determining the rate in 1M KOH for the MoS_2@NiO composite nanostructures as shown in Figure 3(b). The Tafel slope for the NiO (46 mV/decade) and the pristine MoS_2 (44 mV/decade) indicates that also these samples follow the Heyrovsky mechanism, and that the reaction rate is limited by the electrochemical desorption of the hydrogen gas. The Tafel slope for the GCE is 105 mV/decade, in which the rate of reaction is limited by the Volmer step and induces slower HER activity in this sample. The Tafel slope of Pt/C noble catalyst is 30 mV/decade, indicating that the electrochemical reaction is limited by adsorption (Tafel step). The values of the Tafel slopes for MoS_2@NiO, NiO and MoS_2 (~40 mV/decade) are relative low, almost one half of the reported Ni-based and other electrocatalysts in the alkaline media, including NiO/Ni-carbon nanotubes (82 mV/decade),[41] Ni_3S_2 nanoparticles (97 mV/decade),[44] CoP nanowires on carbon cloth (129 mV/decade),[37] NiCu nanoalloys (116 mV/decade),[45] Ni-Mo/Cu nanowires (107 mV/decade),[46] and electrodeposited Ni nanoparticles (88 mV/decade).[47] By considering the Tafel slope of the electrocatalyst in this study in alkaline media with respect to reported catalysts, we have produced the best known electrocatalyst (from this point of view) for hydrogen evolution reaction in alkaline media, which is very important for industrial applications. The smaller the Tafel value, the faster is the HER kinetics and the better for hydrogen production.

Most of the studies in the literature on MoS_2-based catalysts for HER use Ni foam and other conducting substrates, which somewhat impairs their validity, since the foam itself is catalytically

active. In the present study, instead, the use of powders deposited on GCE prevents the problem of the Ni foam, improving the reliability of the results. It is generally accepted that Ni-based electrocatalysts can be a basis for the future generation of efficient catalysts in alkaline media. We demonstrated Ni-based composites with efficiencies close to that of benchmarking Ni-based electrocatalysts.[41]

To gain additional information about the HER mechanism, we calculated the electrochemical surface area by simple cyclic voltammetry versus Ag/AgCl (**Figure 4** (a-f)), from the slope of the linear fit of the average current density versus the scan rate. We obtained almost similar values for NiO, MoS_2 and MoS_2@NiO, i.e. $(1.46 \pm 0.02)\times10^{-4}$ F/cm^2 for pure MoS_2, $(1.45\text{E-}4 \pm 0.03)\times10^{-4}$ F/cm^2 for NiO, and $(1.47\text{E-}4 \pm 0.03)\times10^{-4}$ F/cm^2 for MoS_2@NiO. From these results, we can deduce that no significant increase in surface area is found in the composite catalysts. The improvement in HER activity should come from the synergetic effects between MoS_2 and NiO nanostructures in the composite form and not from an increase in specific surface area.

Figure 5(a) shows the HER polarization curves of the MoS_2@NiO sample before and after the stability test. The composite catalyst is highly stable, without any current density loss. We performed the stability test through chronopotentiometry for the MoS_2@NiO composite for 13 hours. We found a gradual shift in the voltage from 490 mV to 510 mV to maintain the current density at 10 mA/cm^2 the first two hours, and no potential drop was observed after the two-hour transient for the remaining eleven hours.

Electrochemical impedance spectroscopy was utilized to quantify the surface phenomena and the kinetics of HER on the developed catalysts (**Figure 6**). NiO showed two orders of magnitude higher values of total capacitance (**Figure 6A**) visible at low frequencies in comparison with MoS_2. Consistently, the capacitance of NiO film (**Figure 6B**) visible as ordinate value of transition towards the saturation was two orders of magnitude higher than for MoS2.[48] These effects illustrate the higher concentration of charge carriers in NiO film in comparison with MoS_2. The mutual integration of MoS_2 and NiO led to the monotonous transition of electrocapacitive properties between the pristine films.

The presence of two time-resolved processes visible in the Bode plot (e.g. on the spectra of composite film, **Figure 6E**) was modelled by two RC elements in the simplest unified equivalent circuit (Inset in **Figure 6**) developed for an electrode covered with a damaged (porous) coating [49] Since the boundary between the layers is not ideally smooth, due to increased surface roughness

of the porous film, a quantitative analysis of the electrode impedance response requires a more complicated, distributed circuit model featuring constant phase elements (CPE) rather than pure capacitors. The equivalent circuit (Inset in **Figure 6**) providing the best fit consists of the solution resistance R_s and two combined R-CPE units (I and II). A single set of parameters has been used to simultaneously fit the real and imaginary parts of the impedance over the frequency range from 1.25 Hz to 50 kHz. A value of the fitting quality parameter χ^2 of ≤ 0.001 obtained for all spectra indicates a very good fit. The first R-CPE unit showed smaller RC values than the second one illustrating the faster kinetics of the first process. Therefore, the first R-CPE unit might be assigned to fast electronic transport connected with faradaic phenomena of HER (where R_I – charge transfer resistance proportional to reversed rate constant of electrode reaction, CPE_I – double layer capacitance of GCE at the bottom of pores), while the second R-CPE unit might be assigned to the slower ionic transport (where R_{II} – resistance of the film established via pores, CPE_{II} – film capacitance).[49] Consistently with raw signal evaluation, the NiO film showed a 46 times larger value of capacitance (ca. 46 μF) in comparison with MoS_2 (1 μF), while the composite film showed an intermediate value (3 μF). Coherently, the MoS_2 film showed 4 times lager film resistance than NiO, as shown in **Figure 6D**. The capacitance of double layer established on glassy carbon on the bottom of pores revealed a smaller alteration on different film material (0.8 μF, 4.5 μF and 0.7 μF for MoS_2, NiO and the composite film, respectively) illustrating the minor morphology change at GCE/film interface as shown in **Figure 6E**. Importantly, the NiO film showed a significantly smaller charge transfer resistance (15 Ω) in comparison with pristine MoS_2 and the composite films (4.1 kΩ and 475 Ω, respectively) as shown in **Figure 6C**. This result explains the fastest HER rate on NiO. The composite film revealed a transitional value of HER rate between the two pristine films NiO and MoS_2.

In summary, we developed a novel architecture composed of NiO semiconducting nanostructures covered by a MoS_x layer through the simple excessive sulfurization method, and we tested it for HER in alkaline media. The NiO and MoS_2 in composite structure exhibit cubic and hexagonal crystalline features, respectively. The composite system is purely composed of Ni, O, Mo and S elements with no other impurity. The synthetic strategy is simple and cost effective and can be used at large scale for the production of functional materials. The chemical sulfurization process results in increased density of active sites in the composite catalysts. The hybrid catalyst demonstrated better HER performance (including stability and durability) compared to pristine

MoS_2 electrocatalyst, achieving low overpotential for HER, as demonstrated by the extremely low Tafel slope and high current densities, which has never been reported before for MoS_2-based catalysts in alkaline media. The obtained lowest Tafel slope value (43 mV/decade), the excellent durability and stability are the prominent features of the new nonprecious electrocatalyst and make it a good candidate for precious metal free catalysis in HER. These results can be useful for not only water splitting, but also in a broader range of applications, like for instance oxygen reduction reactions, supercapacitors, lithium ion batteries, gas sensing and fuel cells.

Experimental Methods

Synthesis of NiO nanostructures and their composites with MoS_x.

Nickel chloride hexahydrate, hexamethylenetetramine, ammonium phosphomolydate hydrate, L-cystein, potasium hydroxide, and 5% Nafion were purchased from Sigma Aldrich Stockholm Sweden. All chemicals were of analytical grade and used without further purification.

Synthesis of NiO nanostructures

NiO nanostructures were obtained by two steps. Firstly, nickel hydroxide nanostructures were prepared by mixing 2.37 g of nickel chloride hexahydrate and 1.41 g of hexamethylenetetramine in 100 mL of distilled water. A homogenous solution was obtained by constant stirring for 30 mints. Then growth solution was covered with an aluminum foil and left into preheated electric oven at 95 °C for 5 hours. After the completion of growth time, nickel hydroxide nanostructures were obtained by filtration and followed by washing several times with deionized water and dried at room temperature for overnight. In the second step, nickel hydroxide phase was converted into NiO by calcination at 450 °C in air for 3 hours.

Synthesis of MoS_2@NiO composite nanostructures

After the growth of Ni oxide nanostructures, the MoS_x layer was deposited on them. A quantity of 0.3 grams of NiO nanomaterial was immersed in the growth solution of 0.175 g ammonium phosphomolybdate hydrate and 0.275 g of L-cystein in 50 mL of distilled water, each in a separate Teflon vessel of capacity of 100 mL. The Teflon vessel was sealed in a stainless-steel autoclave at 200 °C for 20 hours. A thick layer of MoS_x was deposited on nickel oxides, giving the final structure of the composite materials.

Characterization.

The morphology of nanostructures was evaluated by JEOL scanning electron microscope (SEM) operated at 15 KV. The crystalline structure and phase purity of pristine NiO and MoS2@NiO composite nanostructures was investigated by X-ray powder diffraction using a Philips powder diffractometer associated with CuKα radiation (λ = 1.5418 Å) at generator voltage of 45 kV and a current of 45 mA. The X-ray photoelectron spectroscopy (XPS) experiments were performed using a Scienta ESCA 200 spectrometer in ultrahigh vacuum at a base pressure of 10^{-10} mbar with a monochromatic Al (K alpha) x-ray as a source of photons with 1486.6 eV. The XPS experimental methodology was set in such a way so that the full width at half maximum of the clean Au 4f7/2 line was 0.65 eV. All spectra were obtained at a photoelectron takeoff angle of 0° (normal

emission). All the samples for HRTEM and STEM were prepared via a mechanical process, as published elsewhere. [S1] HRTEM and STEM images have been collected through a FEI Tecnai F20 field emission gun microscope with a 0.19 nm point-to-point resolution at 200 kV equipped with an embedded Quantum Gatan Image Filter for EELS analyses. The collected images were analyzed by means of Gatan Digital Micrograph software.

Electrolysis of water in alkaline media.

All HER experiments were carried on a Solartron analytical potentiostat using three-electrode system cell assembly in 1M KOH solution saturated with N_2 gas. The catalyst ink was prepared by 10 mg of each catalyst in 2 mL of distilled water and 100 µL of 5% Nafion and mixture was sonicated in ultrasonic bath for 15 mints in order to get a homogenous catalyst ink. A glassy carbon electrode (3 mm in diameter) was applied as working electrode for deposition of 10 µL of catalysts ink by drop casting method and used as working electrode. The modified glassy carbon electrode was dried with flow of N_2 gas at room temperature. An Ag/AgCl with saturated KCl as reference electrode and platinum mesh was used as counter electrode respectively. Linear sweep voltammetry was employed at the scan rate of 5 mV/s for HER characterization in alkaline media. Electrochemical Impedance Spectroscopy (EIS) experiment was performed in the frequency range of 50 kHz to 1.25 Hz with onset potential of 100 mV and an amplitude of 10 mV at the reference. The capacitance double layer was used to estimate active surface area by cyclic voltammetry against Ag/AgCl. The potential vs RHE was calibrated to RHE through Nernst equation. $E_{RHE} = E_{Ag/AgCl} + 0.059pH + E^{o}_{Ag/AgCl}$.

Acknowledgements.

AV and ZHI acknowledge Knut and Alice Wallenberg Foundation and Kempe Foundation for partial funding. JA and PYT acknowledge funding from Generalitat de Catalunya 2017 SGR 327 and the Spanish MINECO project VALPEC (ENE2017-85087-C3). ICN2 acknowledges support from the Severo Ochoa Programme (MINECO, Grant no. SEV-2013-0295). ICN2 and IREC are funded by the CERCA Programme / Generalitat de Catalunya. Part of the present work has been performed in the framework of Universitat Autònoma de Barcelona Materials Science PhD program.

Figure Captions

Figure 1. (a, b) SEM images of the nickel oxide nanostructures before (a) and after (b) deposition of the MoS_x layer, respectively. (c, d) XRD patterns of bare NiO (c) and MoS_2@NiO (d) nanostructures. (e) XPS S2p core level spectra and (f) S2s and Mo3d core level spectra of the MoS_2@NiO composite. In (e) and (f) the measured spectra are represented by dots, while the dashed and solid lines are fitting curves.

Figure 2. (a) EELS chemical composition maps obtained from the red rectangled area of the ADF-STEM micrograph. Individual Ni (red), O (green) maps and their composite, (b) Left Top: low magnification TEM image showing the nanostructure. Right top: the magnified HRTEM image shows the detail parts of left top TEM. Left bottom: HRTEM micrograph showing the twin boundary located at the red squared region and the corresponding FFT spectrum indicates that the material crystallizes in the cubic NiO phase. Right bottom: HRTEM image showing the detailed structure of the blue squared region, which is also visualized from the [101] direction, as confirmed by the FFT spectrum. (c) EELS chemical composition maps obtained from the red rectangle area of the ADF-STEM micrograph for the NiO/MoSx composite. Individual element maps and their composites are reported, (d) NiO/MoSx system. Left top: low magnification TEM image showing the distribution of the NiO/MoS_x nanocomposite. Middle and Right top: HRTEM micrograph showing the structure of the NiO nanoplate. Left bottom: HRTEM image of the red squared region and the corresponding FFT spectrum. Right bottom: detailed structure of the interface of the blue squared region and the corresponding FFT spectrum.

Figure 3. (a) Linear sweep voltammetry (LSV) HER polarization curves in N_2 saturated 1M KOH at 25 °C. (b) Calculated Tafel slopes for the different samples.

Figure4. (a-f). Electrochemical surface area estimated by cyclic voltammetry (a, c, e) against Ag/AgCl as reference electrode in 1M KOH saturated with N_2 gas, and linear fit (b, d, f) for pure NiO (a, b), pure MoS_2 (c, d) and MoS_2@NiO (e, f).

Figure 5. (a) HER polarization curves before and after 13 hours stability test in alkaline media. (b) Chronopotentiometry stability in alkaline media for 13 hours at the current density of 10 mA/cm^2.

Figure 6. A. The effect of film composition on total capacitance, 6B. The frequency dependencies of the total capacitance calculated from impedance spectra acquired on pristine (MoS_2 and NiO as black and blue, respectively) and a composite films (red); onset potential of HER (100 mV), 10 mV amplitude, 1M KOH, 6C Impedance spectra acquired on pristine (MoS_2 and NiO as black and blue, respectively) and a composite films (red); solid lines – results of the fitting with equivalent circuit (Inset in D-E); onset potential of HER (100 mV), 10 mV amplitude, 1M KOH.

Figure 1

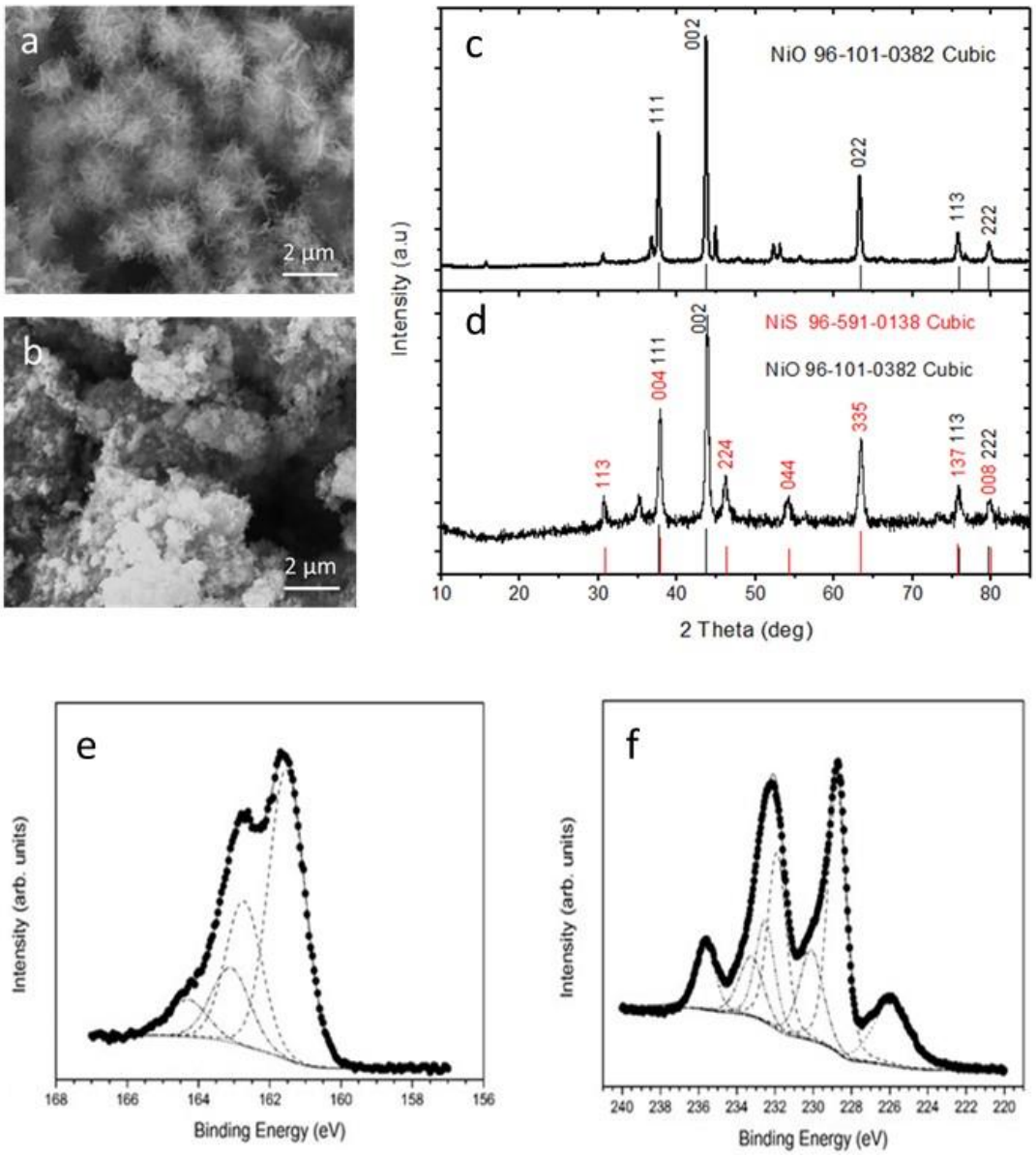
a
2 µm
b
2 µm
c
NiO 96-101-0382 Cubic
002
111
022
113
222
d
NiS 96-591-0138 Cubic
NiO 96-101-0382 Cubic
004 111
002
113
224
044
335
137 113
008 222
Intensity (a.u)
10 20 30 40 50 60 70 80
2 Theta (deg)
e
Intensity (arb. units)
168 166 164 162 160 158 156
Binding Energy (eV)
f
Intensity (arb. units)
240 238 236 234 232 230 228 226 224 222 220
Binding Energy (eV)

Figure 2

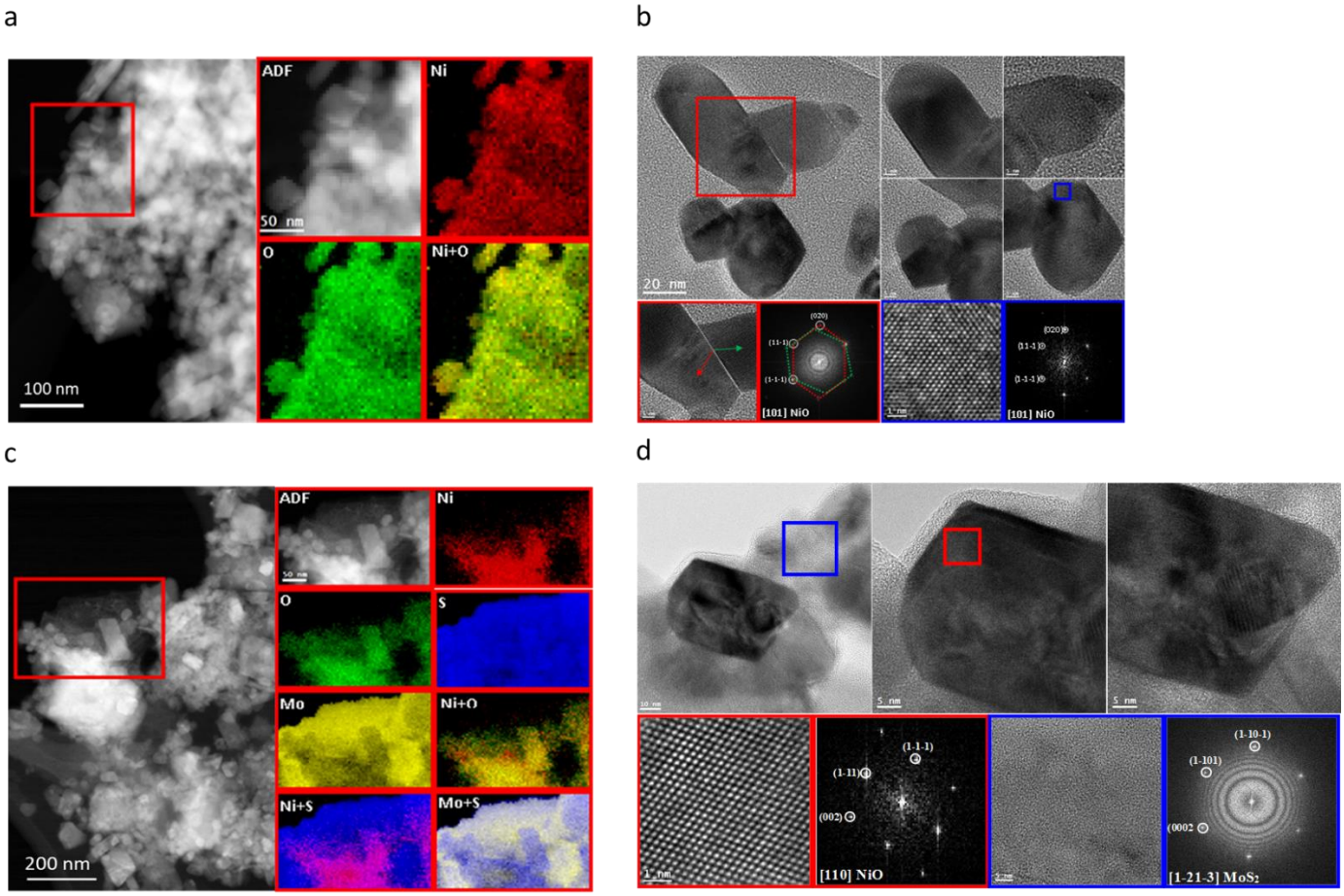
a
ADF
Ni
50 nm
O
Ni+O
100 nm
b
20 nm
(020)
(11-1)
(1-1-1)
[101] NiO
(020)
(11-1)
(1-1-1)
[101] NiO
c
ADF
Ni
O
S
Mo
Ni+O
Ni+S
Mo+S
200 nm
d
5 nm
5 nm
(1-1-1)
(1-11)
(002)
[110] NiO
(1-10-1)
(1-101)
(0002)
[1-21-3] MoS2

Figure 3

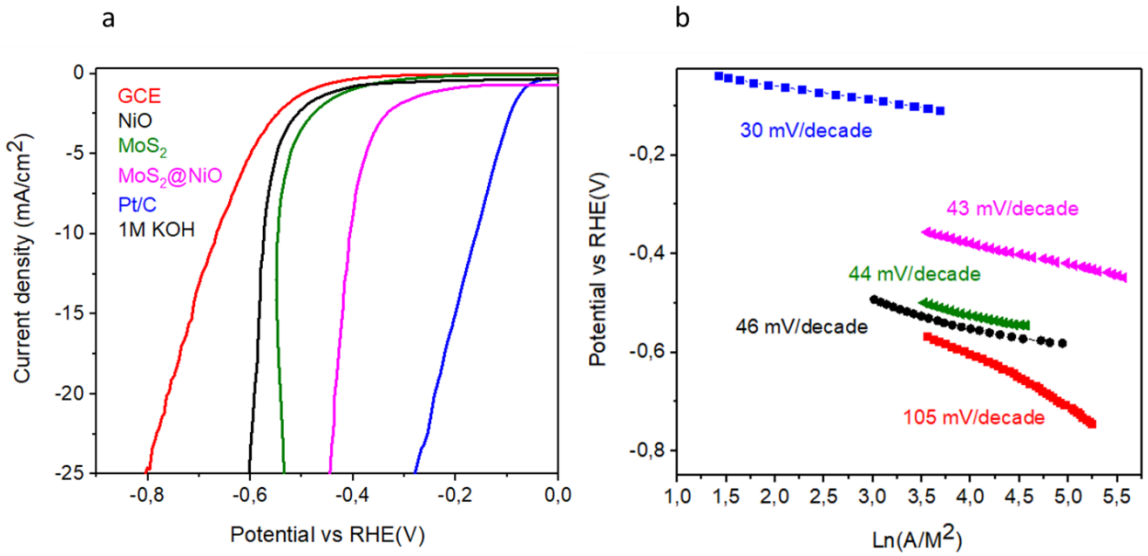
a
b
GCE
NiO
MoS2
MoS2@NiO
Pt/C
1M KOH
Current density (mA/cm2)
Potential vs RHE(V)
0
-5
-10
-15
-20
-25
-0,8
-0,6
-0,4
-0,2
0,0
30 mV/decade
43 mV/decade
44 mV/decade
46 mV/decade
105 mV/decade
Potential vs RHE(V)
Ln(A/M2)
-0,2
-0,4
-0,6
-0,8
1,0
1,5
2,0
2,5
3,0
3,5
4,0
4,5
5,0
5,5

Figure 4

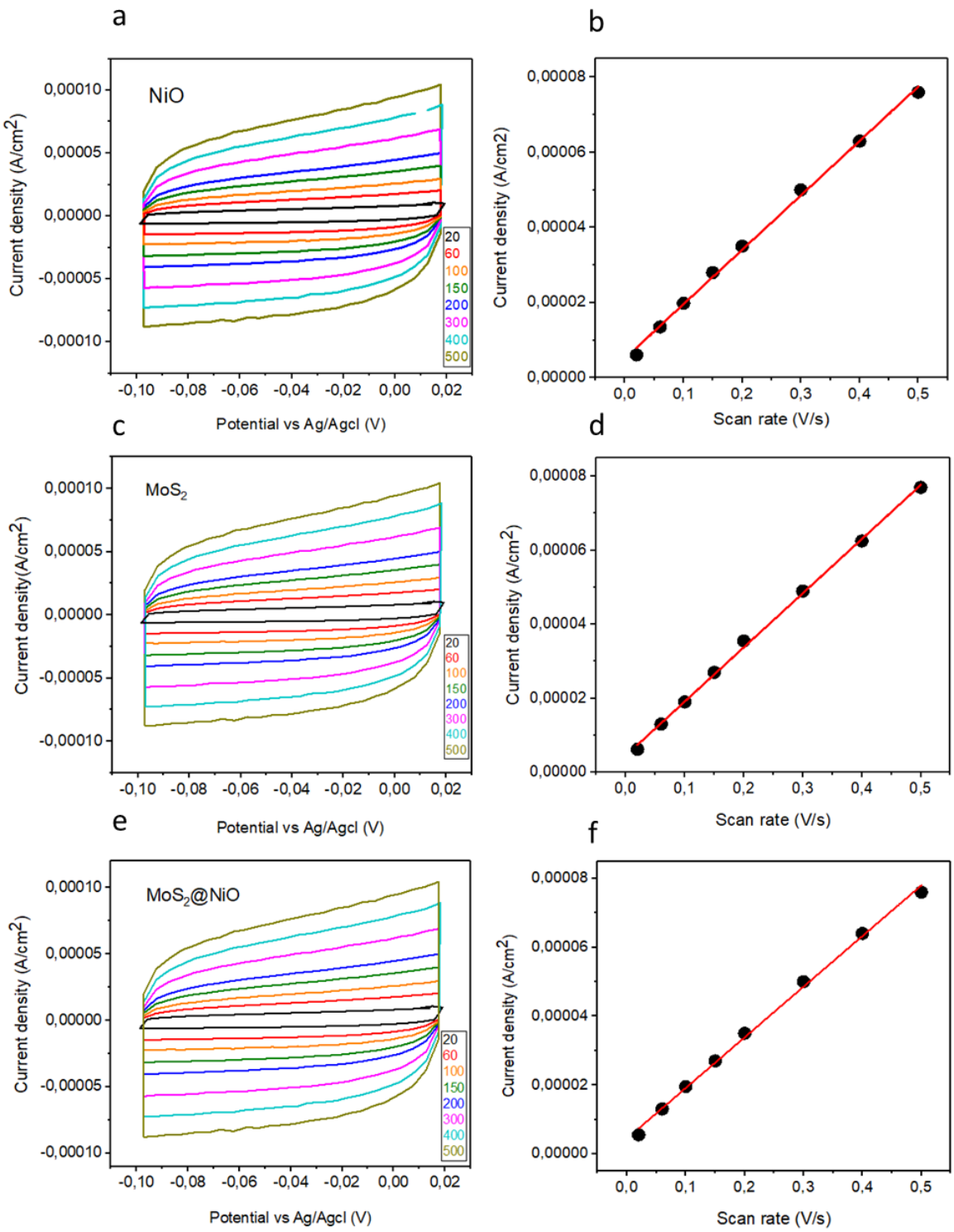
a
NiO
Current density (A/cm2)
Potential vs Ag/Agcl (V)
20
60
100
150
200
300
400
500
b
Current density (A/cm2)
Scan rate (V/s)
c
MoS2
Current density(A/cm2)
Potential vs Ag/Agcl (V)
d
Current density (A/cm2)
Scan rate (V/s)
e
MoS2@NiO
Current density (A/cm2)
Potential vs Ag/Agcl (V)
f
Current density (A/cm2)
Scan rate (V/s)

Figure 5

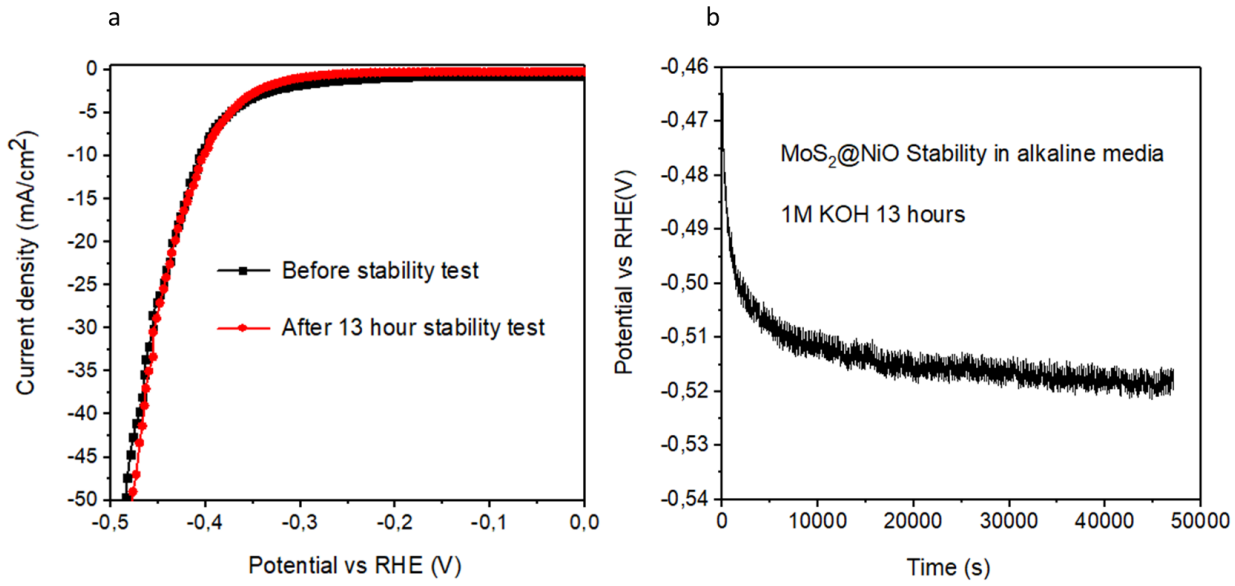
a
b
Current density (mA/cm2)
Potential vs RHE (V)
Before stability test
After 13 hour stability test
Potential vs RHE(V)
Time (s)
MoS2@NiO Stability in alkaline media
1M KOH 13 hours

Figure 6

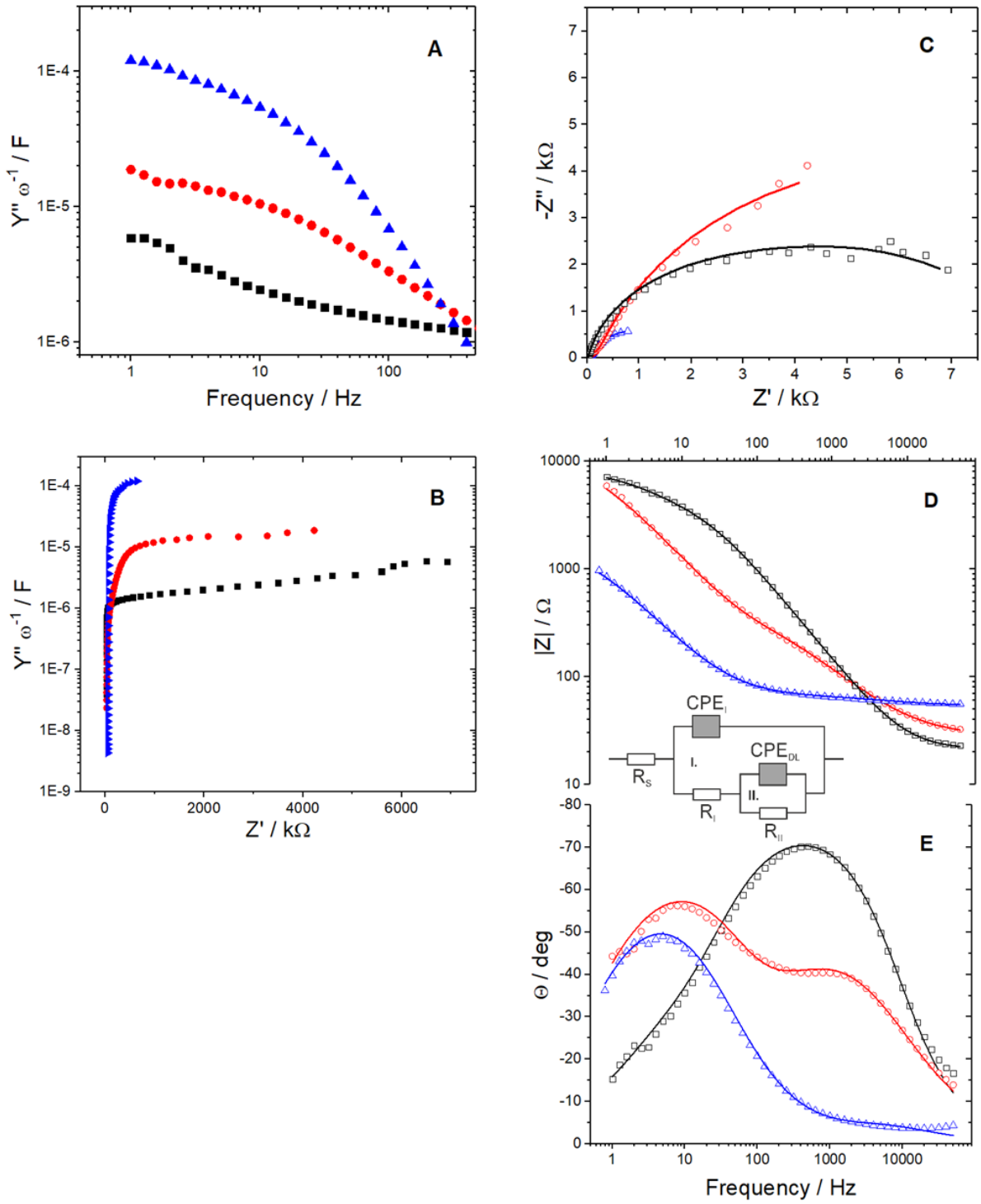
A
Y'' ω-1 / F
1E-4
1E-5
1E-6
1
10
100
Frequency / Hz
C
-Z'' / kΩ
Z' / kΩ
B
Y'' ω-1 / F
1E-4
1E-5
1E-6
1E-7
1E-8
1E-9
0
2000
4000
6000
Z' / kΩ
D
|Z| / Ω
CPEI
CPEDL
RS
RI
RII
I.
II.
E
Θ / deg
Frequency / Hz

MoS_2@NiO composite nanostructures: an advanced nonprecious catalyst for hydrogen evolution reaction in alkaline media

Zafar Hussain Ibupoto[a, b*], Aneela Tahira[a], PengYi Tang[c,d], Xianjie Liu[e], Joan Ramon Morante[d], Mats Fahlman[e], Jordi Arbiol[c,f], Mikhail Vagin[e], Alberto Vomiero[a*]

[a] Division of Material Science, Department of Engineering Sciences and Mathematics, Luleå University of Technology, 97187 Luleå, Sweden

[b] Dr. M.A Kazi Institute of Chemistry University of Sindh Jamshoro, 76080, Sindh Pakistan

[c] Catalan Institute of Nanoscience and Nanotechnology (ICN2), CSIC and BIST, Campus UAB, Bellaterra, 08193 Barcelona, Catalonia, Spain

[d] Catalonia Institute for Energy Research (IREC), Jardins de les Dones de Negre 1, Sant Adrià del Besòs, Barcelona 08930, Catalonia, Spain

[e] Department of Physics, Chemistry and Biology, Linkoping University, 58183 Linkoping, Sweden

[f] ICREA, Pg. Lluís Companys 23, 08010 Barcelona, Catalonia, Spain

* Corresponding authors: Zafar Hussain Ibupoto, Alberto Vomiero
Email: alberto.vomiero@ltu.se, zafar.ibupoto@ltu.se

Supporting information

Table S1. Elemental atomic composition for NiO/MoS_x films obtained from XPS survey scans.

	Mo	S	O		Ni	
NiO/MoSx	26.5%	34%	36.5%		3%	

Table S2. Curve fitting parameters obtained for the S2p core level of NiO/MoS_x films. A Shirley background and mixed Gaussian/Lorentzian functions were used with the $\Delta(2p_{3/2}\text{-}2p_{1/2})$ kept at 1.2 eV and the intensity ratio at 2:1.

	$S2p_{3/2}$ (#1)	Rel. Conc. (#1)	$S2p_{3/2}$ (#2)	Rel. Conc. (#2)
$NiOMoS_x$	161.5 eV	78%	163.1 eV	22%

Table S3. Curve fitting parameters obtained for the S2s and Mo3d core levels of, NiO/MoS_x films. A Shirley background and mixed Gaussian/Lorentzian functions were used with the $\Delta(3d_{5/2}\text{-}2d_{3/2})$ kept at 3.13 eV and the intensity ratio at 3:2.

	#1		#2		#3		
	$Mo3d_{5/2}$	Rel. Conc.	$Mo3d_{5/2}$	Rel. Conc.	$Mo3d_{5/2}$	Rel. Conc.	S2s
$NiOMoS_x$	228.8 eV	54%	230.1 eV	24%	232.5 eV	22%	225.9 eV

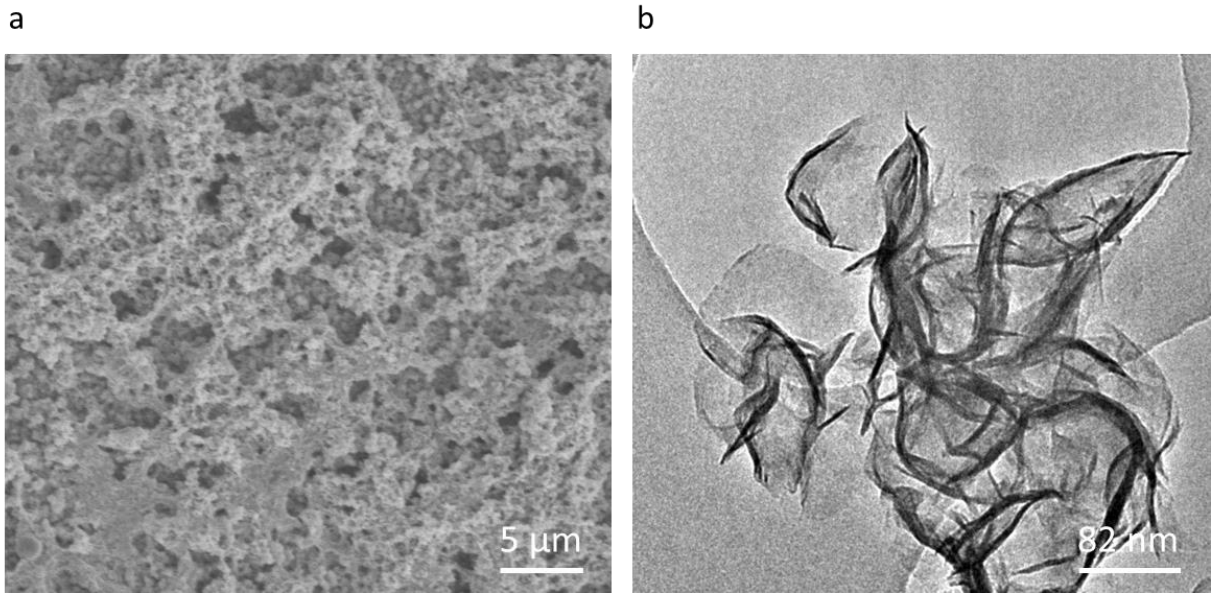

Figure S1: SEM (a) and TEM (b) images of pristine MoS_2.

References

1 J. A. Turner, *Science*. 2004, **305**, 972-974.

2 J. Wang, W. Cui, Q. Liu, Z. Xing, A. M. Asiri and X. Sun , *Adv. Mater*. 2016, **28**, 215-230.

3 M. G. Walter, E. L. Warren, J. R. McKone, S. W. Boettcher, Q. Mi, E. A. Santori and N. S. Lewis, *Chemical Reviews.* 2010, **110**, 6446-6473.

4 Y. Zheng, Y. Jiao, Y. Zhu, L. H. Li, Y. Han, Y. Chen, A. Du, M. Jaroniec and S. Z. Qiao, *Nature Communications.* 2014, **5**, 3783.

5 V. R. Stamenkovic, B. S. Mun, M. Arenz, K. J. J. Mayrhofer, C. A. Lucas, G. Wang, P. N. Ross and N. M. Markovic, *Nat Mater.* 2007, **6**, 241-247.

6 E. A. Hernández-Pagán, N. M. Vargas-Barbosa, T. Wang, Y. Zhao, E. S. Smotkin and T. E. Mallouk, *Energy & Environmental Science.* 2012, **5**, 7582-7589.

7 J.-S. Li, Y. Wang, C.-H. Liu, S.-L. Li, Y.-G. Wang, L.-Z. Dong, Z.-H. Dai, Y.-F. Li, Y.-Q. Lan, *Nature Communications.* 2016, **7**, 11204.

8 H. B. Wu, B. Y. Xia, L. Yu, X.-Y. Yu and X. W. (D) Lou, *Nature Communications.* 2015, **6**, 6512.

9 Y. Zhao, K. Kamiya, K. Hashimoto and S. Nakanishi, *Journal of the American Chemical Society*. 2015, **137**, 110-113.

10 F.- X. Ma, H. B. Wu, B. Y. Xia, C.- Y. Xu and X. W. (David) Lou, *Angewandte Chemie International Edition.* 2015, **54**, 15395-15399.

11 L. Liao, S. Wang, J. Xiao, X. Bian, Y. Zhang, M. D. Scanlon, X. Hu, Y. Tang, B. Liu and H.H. Girault, *Energy & Environmental Science.* 2014, **7**, 387-392.

12 D. H. Youn, S. Han, J. Y. Kim, J. Y. Kim, H. Park, S. H. Choi and J. S. Lee, *ACS Nano.* 2014, **8**, 5164-5173.

13 L. Ma, L. R. L. Ting, V. Molinari, C. Giordano and B. S. Yeo, *Journal of Materials Chemistry A.* 2015, **3**, 8361-8368.

14 H. Wang, C. Tsai, D. Kong, K. Chan, F. Abild-Pedersen, J. K. Nørskov and Y. Cui, *Nano Research. 2015,* **8**, 566-575.

15 M.-R. Gao, J.-X. Liang, Y.-R. Zheng, Y.-F. Xu, J. Jiang, Q. Gao, J. Li and S.-H. Yu, *Nature Communications.* 2015, **6**, 5982.

16 D. Merki and X. Hu, *Energy & Environmental Science.* 2011, **4**, 3878-3888.

17 W. Cui, N. Cheng, Q. Liu, C. Ge, A. M. Asiri and X. Sun, *ACS Catalysis*. 2014, **4**, 2658-2661.

18 W.-F. Chen, C.-H. Wang, K. Sasaki, N. Marinkovic, W. Xu, J. T. Muckerman, Y. Zhu and R. R. Adzic, *Energy & Environmental Science*. 2013, **6**, 943-951.

19 M. Seol, D. H. Youn, J. Y. Kim, J.- W. Jang, M. Choi, J. S. Lee and K. Yong, *Advanced Energy Materials*. 2014, **4**, 1300775-n/a.

20 B. Hinnemann, P. G. Moses, J. Bonde, K. P. Jørgensen, J. H. Nielsen, S. Horch, I. Chorkendorff and J. K. Nørskov, *Journal of the American Chemical Society*. 2005, **127**, 5308-5309.

21 H.I. Karunadasa, E. Montalvo, Y. Sun, M. Majda, J. R. Long and C. J. Chang, *Science*. 2012, **335**, 698-702.

22 J. Kibsgaard, Z. Chen, B.N. Reinecke and T.F. Jaramillo, *Nat Mater*. 2012, **11**, 963-969.

23 M. A. Lukowski, A. S. Daniel, F. Meng, A. Forticaux, L. Li and S. Jin, *Journal of the American Chemical Society*. 2013, **135**, 10274-10277.

24 D. Kong, H. Wang, J. J. Cha, M. Pasta, K. J. Koski, J. Yao and Y. Cui, *Nano Letters*. 2013, **13**, 1341-1347.

25 D. Merki, S. Fierro, H. Vrubel and X. Hu, *Chemical Science*. 2011, **2**, 1262-1267.

26 H. Vrubel, D. Merki and X. Hu, *Energy & Environmental Science*. 2012, **5**, 6136-6144.

27 J. D. Benck, Z. Chen, L. Y. Kuritzky, A. J. Forman and T. F. Jaramillo, *ACS Catalysis*. 2012, **2**, 1916-1923.

28 L. Liao, J. Zhu, X. Bian, L. Zhu, M. D. Scanlon, H. H. Girault and B. Liu, *Advanced Functional Materials*. 2013, **23**, 5326-5333.

29 Y. Li, H. Wang, L. Xie, Y. Liang, G. Hong and H. Dai, *Journal of the American Chemical Society*. 2011, **133**, 7296-7299.

30 Z. Chen, D. Cummins, B. N. Reinecke, E. Clark, M. K. Sunkara and T. F. Jaramillo, *Nano Letters*. 2011, **11**, 4168-4175.

31 T. Wang, L. Liu, Z. Zhu, P. Papakonstantinou, J. Hu, H. Liu and M. Li, *Energy & Environmental Science*.2013, **6**, 625-633.

32 H. Li, C. Tsai, A. L. Koh, L. Cai, A. W. Contryman, A. H. Fragapane, J. Zhao, H. S. Han, H. C. Manoharan, F. Abild-Pedersen, J. K. Nørskov and X. Zheng *Nat Mater*. 2016, **15**, 48-53.

33 Y.- F. Xu, M.- R. Gao, Y.- R. Zheng, J. Jiang and S.- H. Yu, *Angewandte Chemie International Edition*.2013, **52**, 8546-8550.

34 D. Voiry, M. Salehi, R. Silva, T. Fujita, M. Chen, T. Asefa, V. B. Shenoy, G. Eda and M. Chhowalla, *Nano Letters*. 2013, **13**, 6222-6227.

35 X. Yang, W. Fu, W. Liu, J. Hong, Y. Cai, C. Jin, M. Xu, H. Wang, D. Yang and H. Chen, *Journal of Materials Chemistry A*. 2014, **2**, 7727-7733.

36 H. Huang, L. Chen, C. Liu, X. Liu, S. Fang, W. Liu and Y. Liu, *Journal of Materials Chemistry A*. 2016, **4**, 14577-14585.

37 J. Tian, Q. Liu, A. M. Asiri and X. Sun, *Journal of the American Chemical Society*. 2014, **136**, 7587-7590.

38 Y. Zheng, Y. Jiao, L. H. Li, T. Xing, Y. Chen, M. Jaroniec and S. Z. Qiao, *ACS Nano*. 2014, ***8***, 5290-5296.

39 Y. Sun, C. Liu, D. C. Grauer, J. Yano, J. R. Long, P. Yang and C. J. Chang, *Journal of the American Chemical Society*. 2013, **135**, 17699-17702.

40 X. Zou, X. Huang, A. Goswami, R. Silva, B. R. Sathe, E. Mikmeková and T. Asefa. Angew Chem Int Ed Engl. 2014, **53**, 4372-6.

41 M. Gong, W. Zhou, M.-C. Tsai, J. Zhou, M.Guan, M.-C. Lin, B. Zhang, Y. Hu, D.-Y. Wang, J. Yang, S. J. Pennycook, B.-J. Hwang and H. Dai, Nat. Commun. 2014, **5**, 4695.

42 Y. F. Xu, M. R. Gao, Y. R. Zheng, J. Jiang and S. H. Yu, Angew. Chem. Int. Ed. 2013, **52**, 8546 –8550.

43 E. J. Popczun, J. R. McKone, C. G. Read, A. J. Biacchi, A. M. Wiltrout, N. S. Lewis and R. E. Schaak, J. Am. Chem. Soc. 2013, **135**, 9267 – 9270.

44 N. Jiang, Q. Tang, M. Sheng, B. You, D.-e. Jiang and Y. Sun, Catal. Sci. Technol. 2016, **6**, 1077 –1084.

45 X.-D.He, F.Xu, F. Li, L. Liu, Y. Wang, N. Deng, Y.-W.Zhu and J.-B. He, Electroanal. Chem. 2017, **799**, 235– 241.

46 S. Zhao, J. Huang, Y. Liu, J. Shen, H. Wang, X. Yang, Y. Zhu and C. Li, J. Mater. Chem. A 2017, **5**, 4207 –4214.

47 S. Tao, F. Yang, J. Schuch, W. Jaegermann and B. Kaiser, ChemSusChem. 2018, **11**, 1 – 12.

48 Z. Algharaibeh and P G. Pickup, Electrochimica Acta, 2013, **93**, 87-92.

49 a) R.D. Armstrong, A.T.A. Jenkins and B.W. Johnson, Corrosion Science. **37**, 1615-1625,
b) M. Donoghue, R. Garrett, V. Datta, P. Roberts and T. Aben, Materials Performance. 2003, **42**, 36-41.